iScience

CellPress
OPEN ACCESS

Article

APOL1 promotes endothelial cell activation beyond the glomerulus

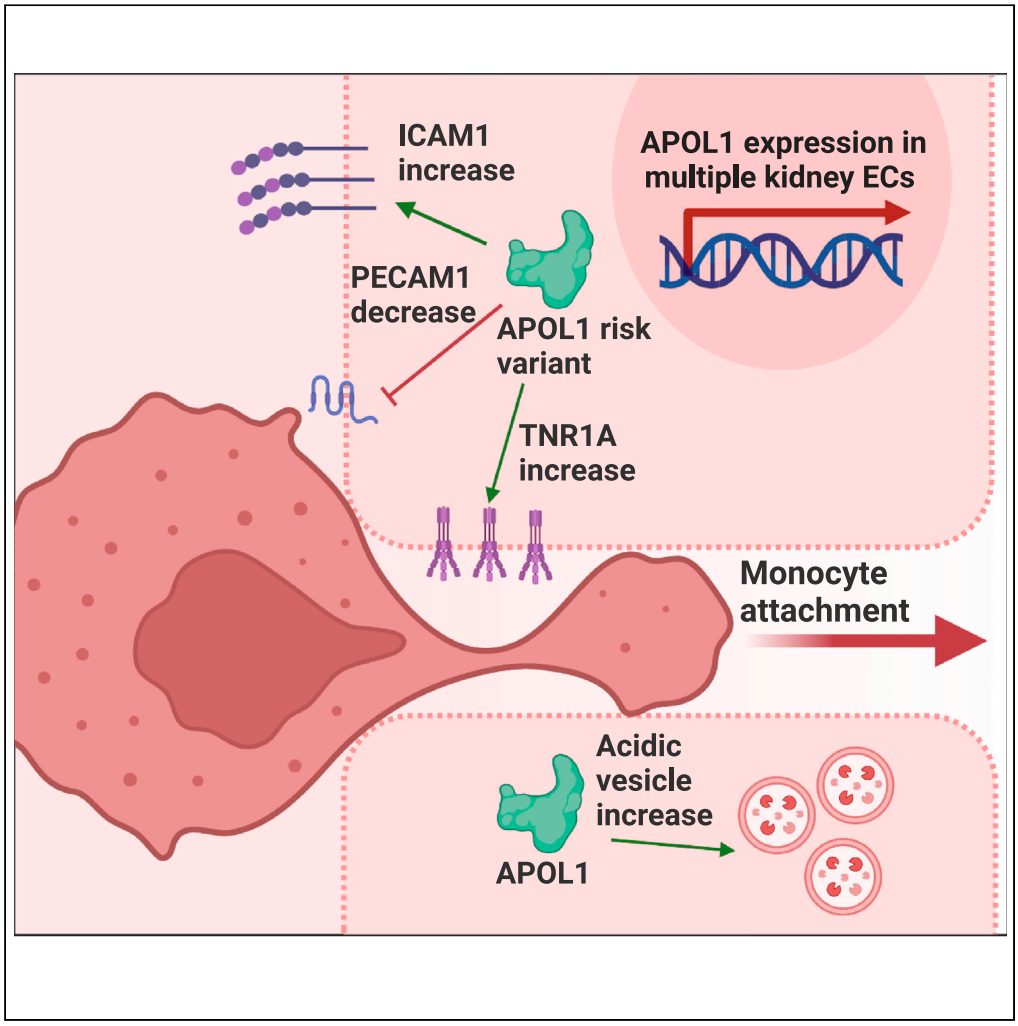

Miguel Carracedo, Elke Ericson, Rasmus Ågren, ..., Alessia Fornoni, Peter J. Greasley, Mark Lal

miguel.carracedoortiz@astrazeneca.com

Highlights

APOL1 is expressed in multiple renal vascular beds

APOL1 is an inducer of endothelial cell (EC) activation in humans

APOL1 RV expression in ECs induces ICAM1 and reduces PECAM1

APOL1 RV expression in ECs promotes monocyte attachment to ECs

Carracedo et al., iScience 26, 106830
June 16, 2023
https://doi.org/10.1016/j.isci.2023.106830

iScience

CellPress
OPEN ACCESS

Article

APOL1 promotes endothelial cell activation beyond the glomerulus

Miguel Carracedo,[1,12,*] Elke Ericson,[2] Rasmus Ågren,[3] Anna Forslöw,[4] Katja Madeyski-Bengtson,[4] Anna Svensson,[4] Rebecca Riddle,[5] Jonas Christoffersson,[6] Hernán González-King Garibotti,[6] Bojana Lazovic,[2,7] Ryan Hicks,[7,8] Lisa Buvall,[1] Alessia Fornoni,[9,10] Peter J. Greasley,[11] and Mark Lal[1]

SUMMARY

Apolipoprotein L1 (APOL1) high-risk genotypes are associated with increased risk of chronic kidney disease (CKD) in people of West African ancestry. Given the importance of endothelial cells (ECs) in CKD, we hypothesized that APOL1 high-risk genotypes may contribute to disease via EC-intrinsic activation and dysfunction.

Single cell RNA sequencing (scRNA-seq) analysis of the Kidney Precision Medicine Project dataset revealed APOL1 expression in ECs from various renal vascular compartments. Utilizing two public transcriptomic datasets of kidney tissue from African Americans with CKD and a dataset of APOL1-expressing transgenic mice, we identified an EC activation signature; specifically, increased intercellular adhesion molecule 1 (ICAM-1) expression and enrichment in leukocyte migration pathways. *In vitro*, APOL1 expression in ECs derived from genetically modified human induced pluripotent stem cells and glomerular ECs triggered changes in ICAM-1 and platelet endothelial cell adhesion molecule 1 (PECAM-1) leading to an increase in monocyte attachment. Overall, our data suggest the involvement of APOL1 as an inducer of EC activation in multiple renal vascular beds with potential effects beyond the glomerular vasculature.

INTRODUCTION

Apolipoprotein L1 (APOL1) is an innate immunity factor expressed only in humans and higher primates, which protects against parasitic infections.[1] Circulating APOL1 is mainly produced in the liver; however, APOL1 is also expressed in several other tissues including kidney. Mutations in the APOL1 gene, known as APOL1 risk variants (RVs), confer resistance against African sleeping sickness. However, these APOL1 RVs, named G1 and G2, are associated with an increased risk of chronic kidney disease.[2,3] G1 and G2 variants present two amino acid substitutions (S342G and I384M) or a two amino acid deletion (388N-389Y), respectively. Histologically, subjects with APOL1-associated nephropathy present with focal segmental glomerulosclerosis and more severe tubulointerstitial fibrosis.[4,5] In accordance with these histopathological findings, APOL1 is predominantly expressed in podocytes and endothelial cells (ECs),[6,7] implying that these cell types may be involved in the development of APOL1-associated kidney disease. In fact, expression of APOL1 RVs in mouse podocytes *in vivo* leads to proteinuria. Overexpression *in vitro* has been associated with mitochondrial alterations,[8,9] endoplasmic reticulum stress,[10] and cell death.[11] In contrast, despite the marked expression of APOL1 in different vascular beds of the kidney,[7] the role of APOL1 RVs in human ECs remains largely unexplored.

The kidney contains a heterogeneous population of ECs with specific structures and functions. Kidney ECs prevent inflammation, control homeostasis and coagulation, maintain vascular tone, and regulate vascular permeability and glomerular filtration. However, activation of the endothelium by inflammatory cytokines, such as interferon (IFN) gamma (IFN-γ) or tumor necrosis factor alpha (TNF), increases the vascular permeability and enhances the expression of adhesion molecules such as intercellular adhesion molecule 1 (ICAM-1) and vascular cell adhesion molecule 1 (VCAM-1), thus favoring the extravasation of inflammatory cells.[12] In addition, IFN-γ and TNF have been shown to increase APOL1 expression in human umbilical vein ECs (HUVECs).[13] In human coronary artery ECs (HCAECs), IFN-γ increases APOL1 expression to a greater extent than in podocytes.[14]

[1]Bioscience Renal, Research and Early Development, Cardiovascular , Renal and Metabolism (CVRM), BioPharmaceuticals R&D, AstraZeneca, Gothenburg, Sweden

[2]Genome Engineering, Discovery Biology, Discovery Sciences, BioPharmaceuticals R&D, AstraZeneca, Gothenburg, Sweden

[3]Translational Science and Experimental Medicine, Research and Early Development, Cardiovascular, Renal and Metabolism (CVRM), BioPharmaceuticals R&D, AstraZeneca, Gothenburg, Sweden

[4]Translational Genomics, Discovery Biology, Discovery Sciences, BioPharmaceuticals R&D, AstraZeneca, Gothenburg, Sweden

[5]Department of Pharmacology, University of Cambridge, Cambridge, UK

[6]Bioscience Cardiovascular, Research and Early Development, Cardiovascular, Renal and Metabolism (CVRM), BioPharmaceuticals R&D, AstraZeneca, Gothenburg, Sweden

[7]BioPharmaceuticals R&D Cell Therapy, Research and Early Development, Cardiovascular, Renal and Metabolism (CVRM), AstraZeneca, Gothenburg, Sweden

[8]School of Cardiovascular and Metabolic Medicine and Sciences, King's College London, London, UK

[9]Katz Family Division of Nephrology and Hypertension, Department of Medicine, Miller School of Medicine, University of Miami, Miami, FL 33136, USA

[10]Peggy and Harold Katz Family Drug Discovery

Continued

Recently, APOL1 RVs have also been associated with the incidence and severity of both acute kidney injury (AKI)[3] and sepsis,[15] conditions characterized by high inflammation and EC activation. Mechanistically, transgenic mice expressing the G2 RV in the endothelium presented moderate proteinuria and increased susceptibility to sepsis, prevented by targeting the inflammasome through NLRP3 inhibition.[15] However, the role of APOL1 as well as the role of the G1 and G2 RVs in human ECs remains largely unexplored. Given the expression of APOL1 in ECs, its inducibility with inflammatory stimuli, and its involvement in sepsis, we aimed to describe the role of APOL1 and its RVs in EC function and activation. To test this, we performed bioinformatic analysis of publicly available datasets and generated novel data using genetically modified ECs derived from i) induced pluripotent stem cells (iPSCs) and ii) primary human glomerular ECs transfected with APOL1-expressing plasmids. Our study highlights that APOL1 RVs promote EC activation, highlighting the importance of ECs in APOL1-mediated nephropathy.

RESULTS

APOL1 is expressed in ECs of the kidney, and its RVs are associated with endothelial activation markers

To better understand the expression profile of *APOL1* in ECs, we analyzed publicly available datasets. Analysis of the kidney precision medicine database (https://doi.org/10.1101/2021.07.28.454201), which contains single-cell transcriptomics of kidney biopsies obtained from healthy, chronic kidney disease (CKD), and AKI subjects, revealed that APOL1 is predominantly expressed in podocytes and ECs from different vascular beds. In contrast, the lowest expressing cells in all groups were dendritic cells, mast cells, and proximal tubule epithelial cells segment ½ (Figures 1A, S1A–S1C, and S2A–S2D). Among the ECs, in all three groups, the highest expression was observed in the cycling ECs, peritubular capillary ECs, afferent/efferent arteriole ECs, and glomerular ECs (Figures 1A and S1A–S1C). However, among the ECs, only glomerular ECs and peritubular capillary ECs showed a significant *APOL1* upregulation in AKI samples when compared to healthy biopsies (Figures 1B, S1D, and S1E).

Analysis of kidney endothelium-specific signature genes and EC activation genes[16] in a dataset from glomerular and tubulointerstitial biopsies, from African Americans with nephrotic syndrome and varied histologic diagnoses[17] contained within the Nephroseq platform, revealed an upregulation of the following genes in the glomerulus: *ICAM1* ($p = 0.014$), insulin-like growth factor 2 (*IGF2*) ($p = 0.015$), endomucin (*EMCN*) ($p = 0.035$), and a trend for *VCAM1* ($p = 0.056$). In contrast, we observed a downregulation of latent transforming growth factor β binding protein 4 (*LTBP4*) ($p = 0.024$) and SPARC-like protein 1 (*SPARCL1*) ($p = 0.037$) when comparing subjects with 0 or 1 RVs (low risk, LR) to those with 2 RVs (high risk, HR) (Figure 1C). In the tubulointerstitial biopsies, *ICAM1* showed a 1.21-fold increase; however, only sclerostin (*SOST*) was significantly upregulated ($p = 0.025$) in the HR biopsies. On the other hand, *SPARCL1* ($p = 0.012$) and platelet EC adhesion molecule (*PECAM1*) ($p = 0.049$) showed a significant downregulation in the HR group (Figure 1C). The increase in EC activation in the glomerulus was replicated in a second cohort, consisting of glomerular RNA sequencing (RNA-seq) from African Americans with focal segmental glomerulosclerosis (FSGS).[18] *ICAM1* was upregulated in HR subjects (Log2 fold change = 0.85, $p_{unadj} = 4.79e\text{-}3$), although not significant after adjusting for multiple testing. Additionally, in the FSGS cohort,[18] *APOL1* expression levels independently of risk status were highly correlated with *ICAM1* expression levels (LR: $\rho = 0.59$, $p = 0.03$; HR: $\rho = 0.53$, $p = 0.04$).

Analysis of a publicly available dataset of transgenic mice expressing APOL1 under a nephrin promoter[19] showed that expression of APOL1 RVs (G1 and G2) led to a significant increase of the endothelial activation markers *ICAM1* and *VCAM1* (Table 1) when compared to mice expressing the G0 variant. Expression of the G1, but not G2 RV, led to a significant decrease in several key endothelial structural genes including *PECAM1*, *CDH5*, and *EHD3* (Table 1). Additionally, VEGFA and its receptors were significantly, and predominantly, downregulated in G1-expressing mice, suggesting an impaired cross talk between podocytes and ECs (Table S1). Pathway analysis revealed leukocyte extravasation to be among the most significant overlapping canonical pathways in both G1 (Z score = 2.524, $p = 1.33E\text{-}05$)- and G2 (Z score = 3.838, $p = 9.96E\text{-}06$)-expressing mice when compared with G0, highlighting the importance of EC activation in this model.

Comparison of the most significant overlapping canonical pathways between LR versus HR in the FSGS patient cohort,[18] G0 versus G1 transgenic mice, and G0 versus G2 transgenic mice revealed an involvement of autophagy and immune cells (Figure 1D). The overlapping biofunctions in all datasets showed an

Center, Miller School of Medicine, University of Miami, Miami, FL 33136, USA

[11]Early Clinical Development, Research and Early Development, Cardiovascular, Renal and Metabolism (CVRM), BioPharmaceuticals R&D, AstraZeneca, Gothenburg, Sweden

[12]Lead contact

*Correspondence: miguel.carracedoortiz@astrazeneca.com

https://doi.org/10.1016/j.isci.2023.106830

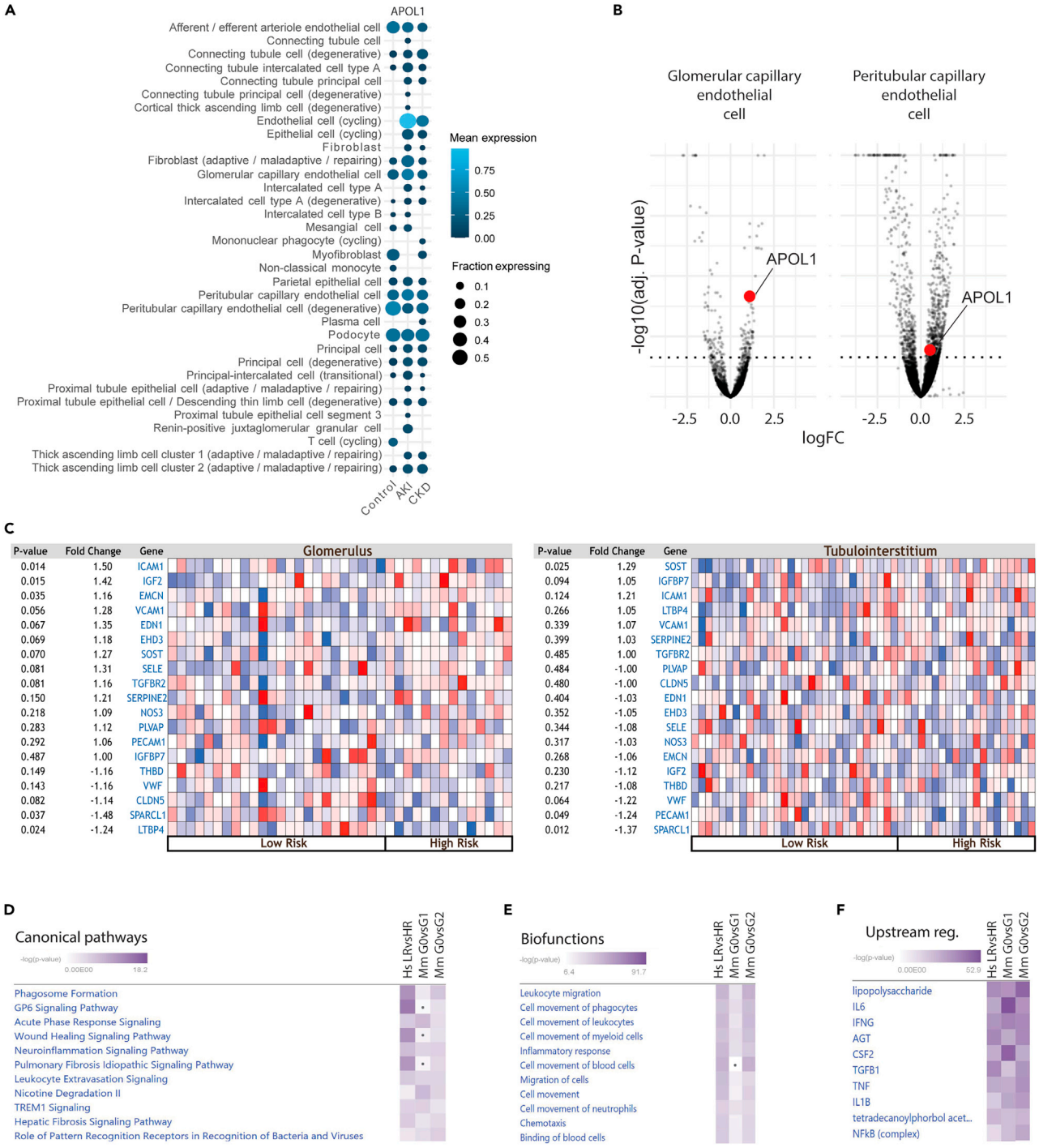

Figure 1. Expression of APOL1 in the kidney and association of APOL1 risk genotypes with EC activation

(A) Mean expression and fraction of cells expressing APOL1 in the single-cell transcriptomics dataset from 43 donors (healthy or with AKI or CKD) within the Kidney Precision Medicine Project (KPMP).

(B) Volcano plot representing APOL1 differential expression between healthy individuals and those with AKI in peritubular capillary endothelial cells (adjusted p value = 0.05 represented by dotted line, APOL1 in red).

(C) Heatmaps showing differential gene expression (log2 fold change) of EC markers from glomerulus (left heatmap) and tubulointerstium (right heatmap) kidney biopsies. Each heatmap shows expression profiles from individuals with nephrotic syndrome and either low-risk or high-risk APOL1 genotypes (see bottom panel).

Figure 1. *Continued*
(D–F) Ingenuity pathway analysis (IPA) illustrating the ranking of the most overlapping canonical pathways (D), biofunctions (E), and upstream regulators (F) between the differentially expressed genes in human glomerular biopsies from LR vs. HR individuals (HsLRvsHR; first column), in transgenic mice overexpressing APOL1 under the nephrin promoter (Mm G0vsG1; second column, and Mm G0vsG2; third column). Dark purple represents high enrichment, whereas white represents low enrichment within the dataset. Round dots depict a non-significant enrichment ($p > 0.01$) of that pathway within the specific dataset.

enrichment in biofunctions associated with immune cell movement and migration (Figure 1E). Moreover, upstream regulator analysis confirmed previously reported inflammatory molecules, such as lipopolysaccharide (LPS), interleukin 6 (IL-6), and IFNγ, as predicted drivers of the transcriptional changes observed in all three groups (Figure 1F). In addition, TNF, a key cytokine driving EC activation and apoptosis linked to APOL1, was also predicted as the top upstream regulator in all three groups. The TNF receptors *TNFRSF1A* and *TNFRSF1B* were both significantly upregulated in G1- and G2-expressing mice compared with G0 counterparts (Table 1).

APOL1 overexpression in iPSCs-derived ECs promotes EC activation

To investigate if EC activation is directly mediated by APOL1 in a cell-specific manner or by systemic factors, we generated stable iPSCs lines expressing APOL1 G0, G1, and G2 under a doxycycline inducible promoter (Figure S3A). Doxycycline stimulation led to significant upregulation of *APOL1* mRNA, to levels comparable with IFN-γ stimulation, and APOL1 protein levels for all three variants (Figures S3B and S3C). We next differentiated these iPSC lines into ECs (Figure 2A) demonstrating expression of key EC markers, VE-cadherin and PECAM1 (Figure S3D). Importantly, these cells also expressed ICAM1, which could be induced by IFN-γ stimulation (Figure S3E).

Gene expression analysis revealed a significant increase in *ICAM1* when the G1 and G2 RVs were expressed following doxycycline stimulation. No increase in *ICAM1* expression was observed in G0 or control iPSC-derived ECs (iECs). G1 and G2 expression also led to a significant decrease in *PECAM1*. Analysis of the chemoattractant molecules C-C motif chemokine ligand 2 and 5 (*CCL2* and *CCL5*) showed a significant decrease in *CCL2* gene expression when APOL1 was induced irrespectively of the variant, while no effect on *CCL5* was seen. *NOS3* expression, a marker of EC health, and *vWF*, a marker of EC activation, showed no significant changes when APOL1 was expressed (Figure 2B). Interestingly, ICAM1 protein expression was significantly increased by G0, G1, and G2 expression following doxycycline stimulation (Figure 2C). In contrast, only G1 led to a significant 18.5% (mean 0.815, 95% confidence interval [CI] 0.71–0.91) reduction in PECAM1 protein levels compared to control (Figure 2D). To test the functional consequences of the observed endothelial activation, we performed a macrophage attachment assay. G1-expressing iECs showed a significant 2.18-fold increase (95% CI 1.21–3.16) in macrophage attachment when compared to both control and G0-expressing cells. G2-expressing iECs showed a 1.52-fold increase (95% CI 1.21–1.83) in macrophage attachment (Figure 2E).

Cell viability remained unaffected after doxycycline stimulation of APOL1 expression despite a decreasing trend by G2 (Figure S4A). Given the effects observed in PECAM1, without changes in viability, we performed a migration assay. iECs expressing APOL1-cDNA showed a decrease in wound closure as compared to doxycycline-treated control iECs (Figure S4B). When compared to each relative control, control iECs showed no effect of doxycycline on wound closure. Doxycycline-induced APOL1 G0 and G2 showed a significant decrease in wound closure. G1 showed a trend for reduced wound closure, which was significant at the last time point.

APOL1 overexpression promotes accumulation of acidic vesicles in iPSCs-derived ECs

EC activation is usually accompanied by changes in cell shape. Analysis of cell area, width, and length by immunofluorescence (IF) showed no significant effect of APOL1 RV expression (Figure 3A). In line with these results, no differences were observed in the forward scatter (FSC) (Figure 3B) when cells were analyzed by flow cytometry; however, APOL1 expression from any risk variant led to a significant increase in the intensity of the side scatter (SSC) (Figure 3B), reflecting changes in cellular complexity.[20] No differences were observed in nuclear size (Figure 3C). However, analysis of acidic vesicles revealed a 1.31 ± 0.07 (95% CI 1.19–1.43), 1.42 ± 0.35 (95% CI 0.86–1.99), and 1.37 ± 0.13 (95% CI 1.16–1.58) fold increase when expressing G0, G1, and G2 respectively (Figure 3D). An increase in acidic vesicles can be a consequence of changes in autophagy. APOL1 RVs have been implicated in mitochondrial alterations.[21] Staining of iECs with a

Table 1. Differential gene expression in transgenic mice expressing APOL1 under a nephrin promoter

	G1vsG0		G2vsG0	
Gene name	Log2FoldChange	p value	Log2FoldChange	p value
VCAM1	4.973	3.50E-51	3.347	4.91E-26
ICAM1	2.828	1.10E-38	1.908	2.83E-18
EDN1	2.897	4.35E-16	1.836	1.39E-07
EHD3	−0.964	2.01E-03	−0.365	3.26E-01
CDH5	−0.752	2.09E-02	0.465	1.87E-01
PECAM1	−0.678	3.23E-02	0.295	4.34E-01
TNFRSF1A	1.342	1.08E-16	0.971	6.01E-09
TNFRSF1B	2.329	3.95E-20	1.95	1.01E-14

mitophagy indicator dye revealed an increase in fluorescence when all APOL1 variants were expressed (Figure 3E). To assess if the increased mitophagy had a functional effect on mitochondrial function, we determined the oxygen consumption rate (OCR). APOL1 expression had no effect on maximal respiration, spare capacity, or OCR (Figure S5A).

APOL1 RVs promote human glomerular EC activation

APOL1 nephropathies are characterized by glomerular alterations. Therefore we studied the role of APOL1 in primary human glomerular ECs (HGECs). Electroporation of HGECs with plasmids containing G0 or G1 variants led to an increase in APOL1 protein levels comparable to those observed in the iPSC-derived ECs (Figure S3F). Gene expression analyses revealed a significant increase in ICAM1 when transiently overexpressing the G1 RV. APOL1 expression, independently of RV, led to a significant decrease in *CCL2*. *NOS3* expression was significantly upregulated with G0 and showed a trend with G1 ($p = 0.12$). In contrast, *vWF* gene expression showed no significant differences when APOL1 was expressed (Figure 4A). However, expression of the G1 RV led to a significant decrease in both gene and protein levels of PECAM1 (Figures 4A and 4B). To test the functional consequences of the observed endothelial activation, we performed a macrophage attachment assay. Addition of macrophages to HGECs transfected with APOL1 G0 and G1 led to a 1.45-fold and 1.72-fold increase in the number of attached macrophages, respectively, when compared to control (Figure 4C).

Additionally, APOL1 G0 overexpression in HGECs led to an increase in apoptotic cells, which was greater with G1 overexpression (Figure 5A). This increase in cell death was accompanied by an increase in caspase 3 and caspase 7 proteins in G1-overexpressing HGECs. Caspase 8 was increased with both G0 and G1 overexpression (Figure 5B). In line with these results, and in accordance with the murine transcriptomics data, overexpression of G1 led to a significant increase of the TNF receptor (TNFR1) protein (Figure 5C). Taken together, analysis of the intracellular complexity of the HGECs replicated the results observed in the iPSC-derived ECs, showing significant increase in acidic vesicles, with higher spot area of punctuae over number of spots, when both G0 and G1 were overexpressed (Figure 5D).

DISCUSSION

In the present study, we show for the first time that APOL1 is an inducer of EC activation in humans. APOL1 expression was observed not only in glomerular ECs but also in peritubular ECs in AKI. APOL1 RV expression in ECs induced adhesion molecules and reduced endothelial junctional proteins, leading to an increase in monocyte attachment. Our results, building on previous work using transgenic mouse models, highlight the importance of ECs, and their relationship with immune cells, as contributors in APOL1-associated nephropathies.

Our results suggest that the role of APOL1 is not restricted to the glomerulus or to the podocytes. In AKI particularly, transcriptomics analysis of small conditional RNA-seq (scRNA-seq) data from KPMC revealed an upregulation in cycling, glomerular, and peritubular ECs. In AKI, APOL1 levels are not only increased in the circulation[15] but also intracellularly in ECs. This preferential increase of *APOL1* transcripts in ECs over podocytes expands previous immunohistochemistry (IHC) and immunofluorescence (IF) results[4,7] and

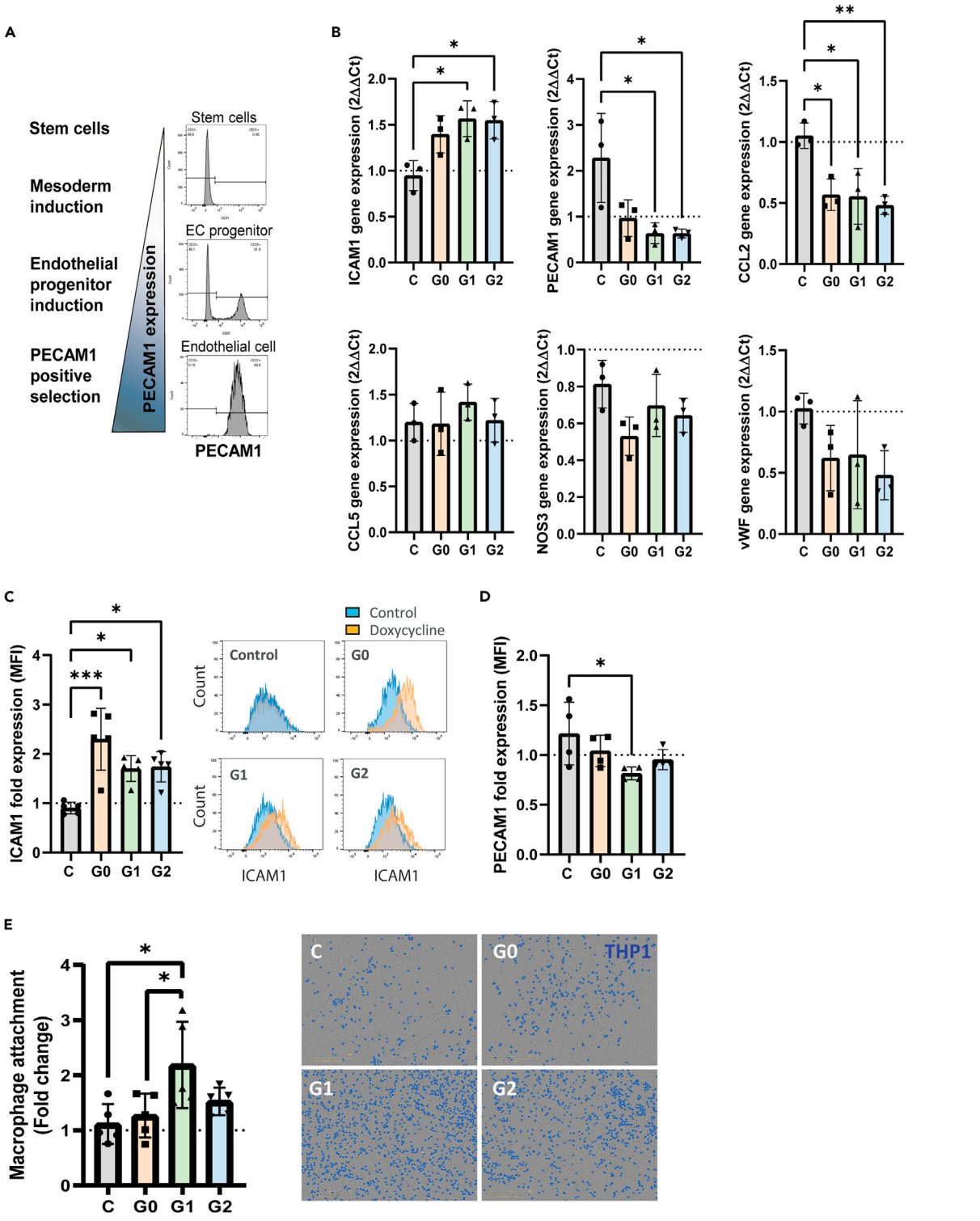

Figure 2. *In vitro* expression of APOL1 iPSC-derived ECs promotes EC activation

(A) Schematic representation of the EC differentiation from iPSCs, and representative histograms of the membrane expression of PECAM1 measured by flow cytometry at selected time points.

(B) Gene expression analysis of key EC markers after APOL1 induction with 1uM doxycycline for 24h.

(C) Membrane protein expression quantification of the adhesion molecule ICAM1 and representative histograms after 24h doxycycline exposure.

(D) Membrane protein expression quantification of the endothelial structural protein PECAM1 after 24h exposure to doxycycline (1uM).

Figure 2. *Continued*

(E) Macrophage adhesion quantification and representative images showing attached macrophages labeled with a cell mask (blue) helping segment the macrophages and allowing quantification.*p < 0.05, **p < 0.01, ***p < 0.001 for one-way ANOVA followed by post hoc test for multiple comparisons. In B, C, D, and E, the results are presented as fold change expression in doxycycline-treated cells compared to non-doxycycline-treated cells. Each dot represents an independent experiment.

confirms earlier *in vitro* findings, showing a greater upregulation of APOL1 by IFN-α, β, and γ in HGECs than in podocytes,[14] supporting a role of APOL1 beyond the podocyte.

In addition, our findings implicate APOL1 RVs as inducers of EC activation, increasing adhesion molecules and enhancing pathways involved in leukocyte migration. In two transcriptomics cohorts,[17,18] HR donors presented an increase in the endothelial activation gene *ICAM1* in the glomerulus. Analysis of a public transcriptomics dataset from transgenic mice expressing APOL1 under the nephrin promoter[19] showed causality between APOL1 RV expression and EC activation and suggested alterations between EC-podocyte cross talk. Importantly, this APOL1-mediated upregulation of EC activation genes does not seem to be constrained to podocytes since overexpression of APOL1-G2 in the endothelium of transgenic mice increases *ICAM1* and *VCAM1*.[15]

However, despite these similarities in EC activation between both mouse models, expression of APOL1 RVs in podocytes[19] leads to greater albuminuria than expression of APOL1-G2 in the endothelium,[15] suggesting that ECs might be more resistant to APOL1 RV overexpression than podocytes. In fact, transgenic expression of APOL1 (G1/G2) in the endothelium of zebrafish promotes endothelial alterations without edema or proteinuria.[22] Nonetheless, this increase in EC activation and alterations in two different mouse models and in zebrafish supports the observed correlation between *ICAM1* and *APOL1* expression levels in the FSGS cohort independently of risk status. Overall, these similarities in EC activation in humans and transgenic mice suggest similar biological pathways are being regulated. In fact, our bioinformatic analysis comparing the transcriptome of human glomeruli with the transcriptome of transgenic mice revealed a strong involvement of pathways associated with immune cell function, specifically pathways related to immune cell migration and extravasation. This relationship between APOL1 RVs and immune cell migration is of particular interest given the recently described association among APOL1 RVs, sepsis,[15,23] and COVID-19.[3,24]

Notably, our *in vitro* results solidified the direct role of APOL1 RVs in EC activation, independently of immune cells. Expression of APOL1 RVs in iPSC-derived ECs and in primary HGECs increased *ICAM1* expression and decreased the endothelial structural protein PECAM1.[25,26] This decrease in PECAM1 aligns with the observed reduction in tubulointerstitial biopsies, as well as with the transgenic mouse transcriptomics data, where G1-expressing mice displayed a decrease in *PECAM1*, *CDH5*, and *EHD3*. In fact, this decrease in endothelial structural proteins may explain the increase in vascular permeability observed by Wu et al., where EC transgenic expression of G2-APOL1 decreased murine *trans*-endothelial electrical resistance *in vitro* and enhanced Evans blue dye leakage in ears.[15] Altogether this suggests that the APOL1 RV-driven loss of endothelial structural proteins may promote vascular permeability and subsequently impact glomerular filtration barrier integrity in APOL1-associated nephropathies.

Macrophage attachment to APOL1-G1-expressing HGECs suggests that expression of APOL1-G1 may promote the recruitment of inflammatory mediators to kidney ECs. In fact, in mouse kidneys after AKI, ECs are among the first cells to signal to leukocytes,[27] and mice lacking EC adhesion molecules are protected from sepsis-induced renal injury.[28] Notably, immune cells from carriers of one or two RVs, with end-stage kidney disease, have shown an enrichment in inflammatory pathways.[29] Collectively this suggests a role for the intercellular relationship between immune cells and ECs in APOL1-associated nephropathies, where ECs may be involved in the initiation of disease and immune cells in the progression.

APOL1 RV expression in more complex models, namely human iPSC-derived ECs, did not cause a decrease in cell viability, suggesting that in this model the APOL1 RV-induced phenotype might be more subtle than in cell lines, requiring a "second hit". In fact, a secondary stressor, namely a scratch wound, led to a decrease in wound closure in APOL1-overexpressing cells. This lack of cell death in non-stressed iPSC-derived cells is consistent with previous data obtained using kidney organoids.[30] In HGECs, cell death was accompanied by an increase in both caspase 8 and TNFR1 in G1-overexpressing HGECs cell, suggesting a potential involvement of Fas-associated protein with death domain (FADD) in the induction of apoptosis. This upregulation of TNFR1 is particularly interesting considering that TNF induces APOL1

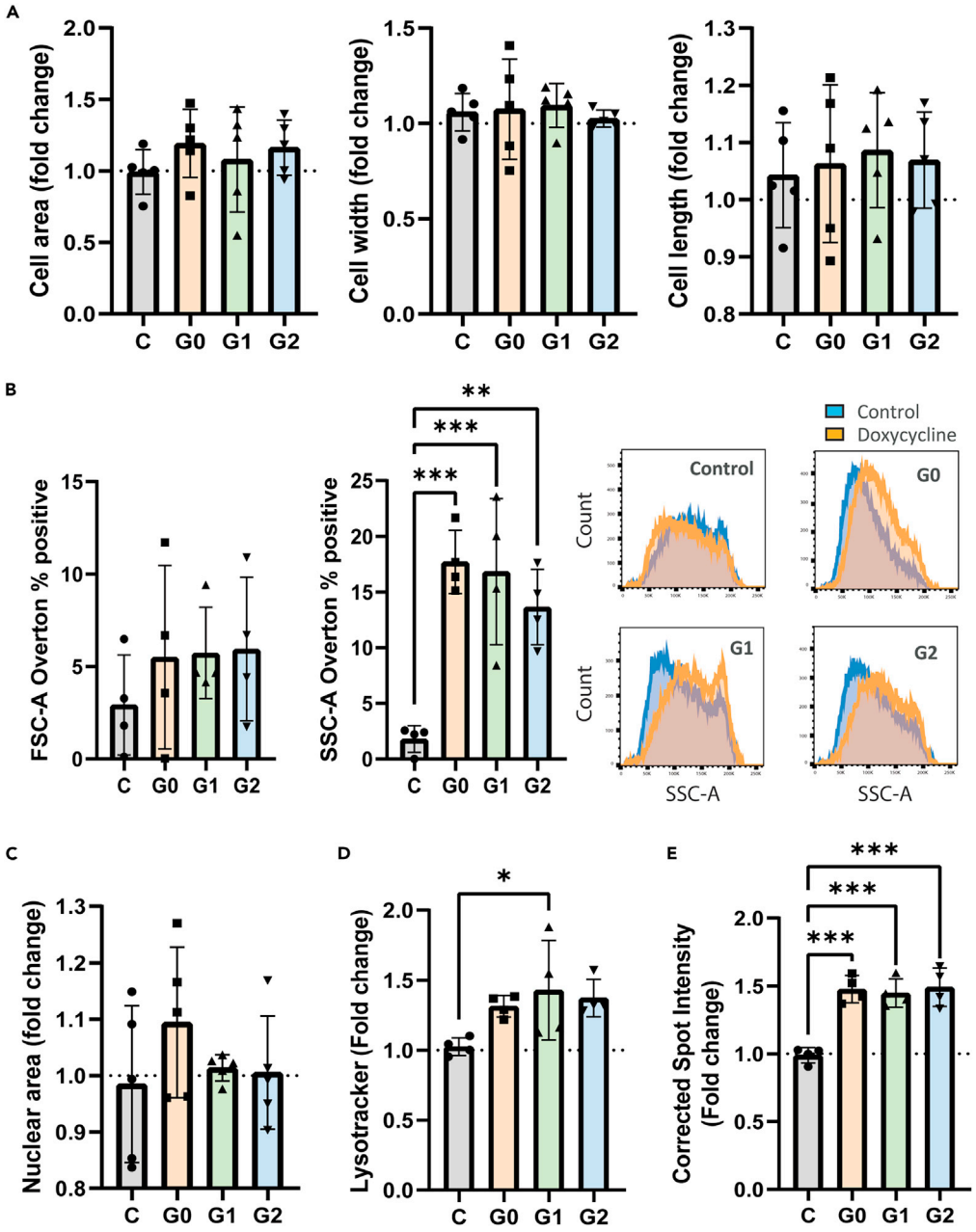

Figure 3. Changes in cellular complexity in APOL1-expressing ECs

(A) Cell morphology quantification by immunofluorescence of ECs.

(B) Effect of APOL1 induction with doxycycline (1uM) for 24h in the forward scatter (FSC) and the side scatter (SSC) normalized against untreated control cells, with representative histograms.

(C) Nuclear size quantification by immunofluorescence of ECs.

(D) Quantification in live cells of acidic organelles by flow cytometry.

(E) Mitophagy assessment in cells pre-loaded with a mitophagy dye for 30min followed by APOL1 induction for 24h, and the fluorescence intensity of punctate quantified. *$p < 0.05$, **$p < 0.01$, ***$p < 0.001$ for one-way ANOVA followed by post hoc test for multiple comparisons. Data presented as fold change to non-doxycycline-treated cells. Each dot represents an independent experiment.

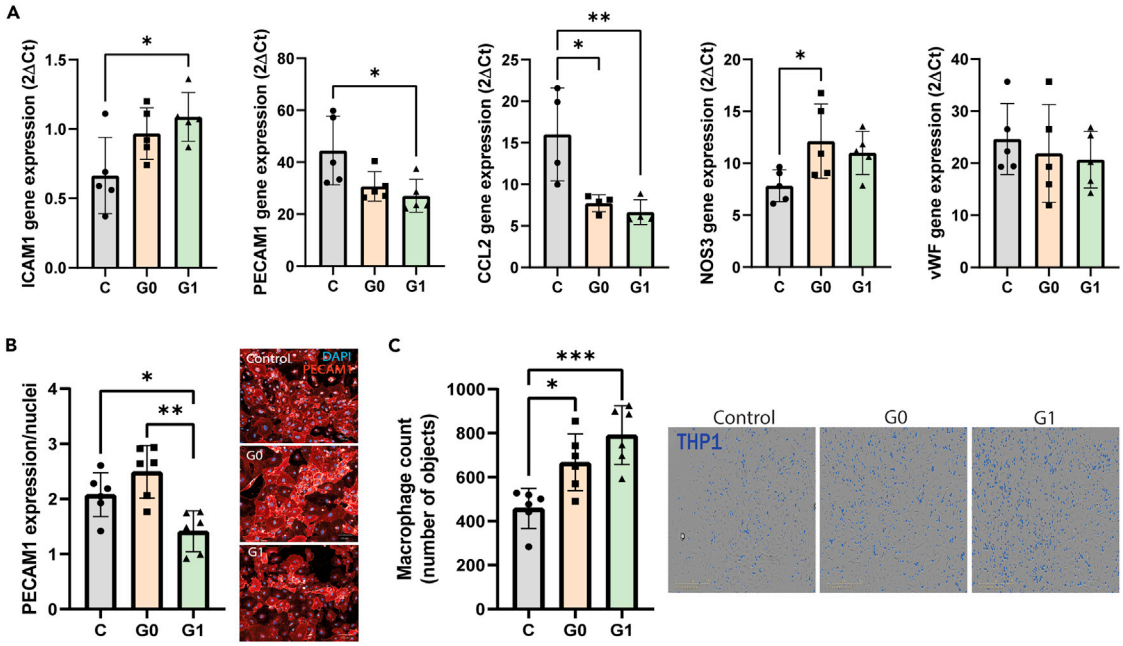

Figure 4. APOL1 RV expression promotes primary glomerular EC activation

(A) Gene expression analysis of key EC markers 24h after electroporation with green fluorescent protein (GFP) plasmid (C), G0 expressing plasmid with a GFP reporter (G0), or G1 expressing plasmid with a GFP reporter (G1).

(B) PECAM1 protein expression quantification 24h after electroporation and representative images.

(C) Macrophage adhesion quantification and representative images showing attached macrophages labeled with a cell mask (blue) helping in segmenting the macrophages and allowing quantification (data representative of three independent experiments). *p < 0.05, **p < 0.01, ***p < 0.001 for one-way ANOVA followed by post hoc test for multiple comparisons. Each dot in the graph represents an independent experiment.

expression.[13] TNF is increased in the serum of LPS-treated G2-overexpresing mice,[15] and plasma concentrations of TNFR1 are independently associated with kidney outcomes in individuals with HR APOL1 genotypes.[31] Moreover, TNF was predicted as an upstream regulator in our bioinformatic analysis. Overall, these data suggest that TNF signaling may act as an upstream regulator in APOL1 pathophysiology.

Finally, APOL1 expression in both iPSC-derived ECs and HGECs led to an increase in intracellular complexity, reflected by an increase in the SSC of these cells. This increase in cellular complexity was accompanied by an increase in acidic vesicles, without changes in mitochondrial bioenergetics, unlike urinary podocytes from donors carrying different APOL1 RVs,[9] suggesting an involvement of APOL1 in the accumulation of lysosomes in ECs. In fact, APOL1 has been shown to increase lysosome accumulation in a dose-dependent manner in 293T cells *in vitro*,[32] and ECs from G2-overerpressing mice present an increase in degradative compartments.[15] Moreover, APOL1 has been shown to promote transcription factor EB (TFEB) nuclear localization and activation of genes relevant for lysosomal biogenesis.[32,33] Overall, it is possible that the APOL1-driven increase in acidic vesicles could be the consequence of an innate immune response. In fact, IFN-mediated viral infections are often characterized by the deposition of electron-dense tubuloreticular inclusions in the kidney endothelium, a characteristic which has frequently been observed in kidney biopsies of African Americans infected with COVID-19.[34–36]

In summary, our work reveals the importance of APOL1 RVs in EC activation and highlights its relevance in multiple vascular beds in humans. Moreover, both our bioinformatic analysis and our *in vitro* work support a relationship between immune cells and ECs in APOL1-associated nephropathies. As a result of APOL1 expression, ECs undergo changes in adhesion molecules, endothelial junctional proteins, inflammatory receptors, and intracellular complexity leading to an increase in monocyte attachment.

Limitations of the study

An important limitation of our study lies on the reliance of *in silico* analyses to explore the expression pattern of APOL1 and the effects of APOL1 RVs in ECs in human tissues without histological evaluation.

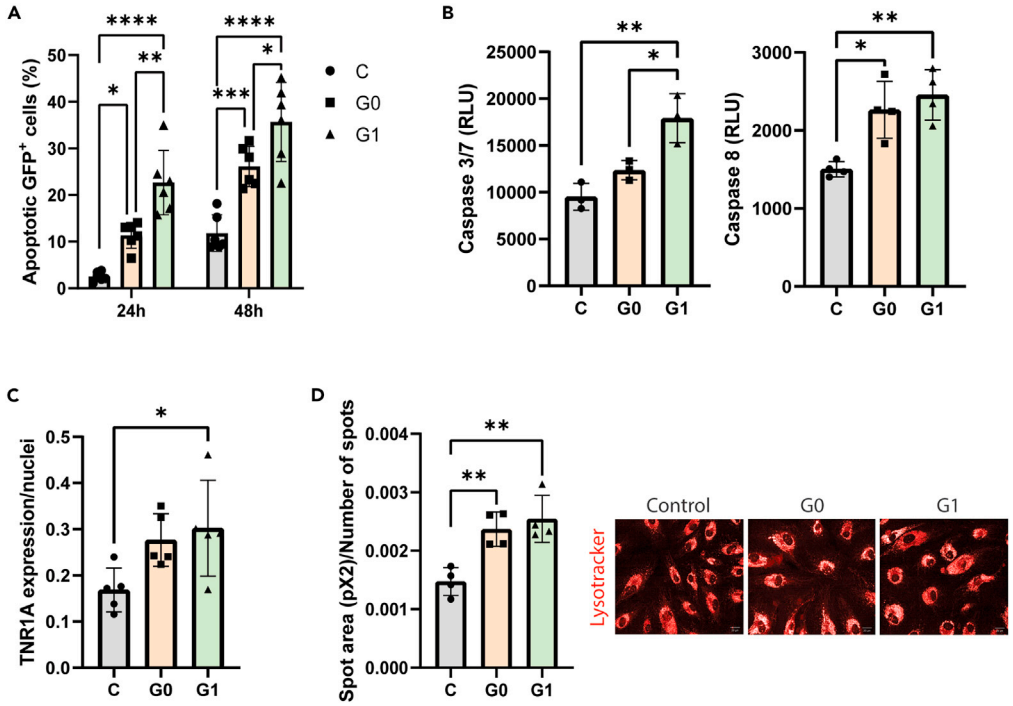

Figure 5. APOL1 RV expression promotes apoptotic pathways in primary glomerular ECs

(A) Cell death in HGECs 24 or 48 h after electroporation, quantified as the percentage GFP cells positive for annexin V staining.

(B) Caspase 3/7 and caspase 8 quantification by luminescence 24h after electroporation.

(C) TNFR1 protein expression quantification 24h after electroporation.

(D) Quantification in live cells of acidic organelles by measuring the spot area of punctate 24h after electroporation.

*p < 0.05, **p < 0.01, ***p < 0.001 for one-way ANOVA followed by post hoc test for multiple comparisons. Each dot in the graph represents an independent experiment.

Future studies shall focus on the histochemical evaluation of APOL1 RV-mediated effects, as well as the assessment of EC injury by electron microscopy in APOL1 HR carriers.

STAR★METHODS

Detailed methods are provided in the online version of this paper and include the following:

- KEY RESOURCES TABLE
- RESOURCE AVAILABILITY
  - Lead contact
  - Materials availability
  - Data and code availability
- MATERIAL AND METHODS
  - Bioinformatic analysis
  - Target vector design inducible ApoL1
- EXPERIMENTAL MODEL AND SUBJECT DETAILS
  - Primary cell cuture
  - Cell line confirmation - Junction PCR
  - Cell line confirmation – ddPCR & sequencing
  - Cell culture and iPSC differentiation to endothelial cells
- METHOD DETAILS
  - Generation of plasmids expressing his-tagged APOL1 and electroporation
  - Immunofluorescence
  - Protein extraction and ELISA

- Gene expression analysis
- Lysotracker labeling
- Macrophage attachment assay
- Mitophagy detection assay
- Flow cytometry analysis
- Oxygen consumption measurements
- Scratch wound assay
- Caspase and cell viability analysis

- QUANTIFICATION AND STATISTICAL ANALYSIS

SUPPLEMENTAL INFORMATION

Supplemental information can be found online at https://doi.org/10.1016/j.isci.2023.106830.

ACKNOWLEDGMENTS

This project has received funding from the European Union's Horizon 2020 research and innovation program under the Marie Skłodowska-Curie grant agreement no. 814316 (B.L.). M.C. was a postdoc fellow of the AstraZeneca R&D postdoc program during this study.

AUTHOR CONTRIBUTIONS

Performed experiments: M.C., E.E., A.F., K.B-M., A.S., J.C., H.K.G., B.L., R.R.

Analyzed data: M.C., R.A., E.E.

Wrote and reviewed manuscript: M.C., E.E., R.A., A.F., K.M-B., A.F., P.J.G., M.L., J.C., H.K.G, B.L., R.R., B.L.

Provided critical input: L.B., A.F., P.J.G., M.L., M.C., R.H.

DECLARATION OF INTERESTS

M.C., E.E., R.A., A.F., K.B-M., A.S., J.C., H.K.G, B.L., R.H., L.B., P.J.G., and M.L. are all AstraZeneca employees.

Received: March 30, 2023
Revised: April 27, 2023
Accepted: May 3, 2023
Published: May 8, 2023

REFERENCES

1. Vanhamme, L., Paturiaux-Hanocq, F., Poelvoorde, P., Nolan, D.P., Lins, L., Van Den Abbeele, J., Pays, A., Tebabi, P., Van Xong, H., Jacquet, A., et al. (2003). Apolipoprotein L-I is the trypanosome lytic factor of human serum. Nature *422*, 83–87. https://doi.org/10.1038/nature01461.

2. Genovese, G., Friedman, D.J., Ross, M.D., Lecordier, L., Uzureau, P., Freedman, B.I., Bowden, D.W., Langefeld, C.D., Oleksyk, T.K., Uscinski Knob, A.L., et al. (2010). Association of trypanolytic ApoL1 variants with kidney disease in African Americans. Science *329*, 841–845. https://doi.org/10.1126/science.1193032.

3. Hung, A.M., Shah, S.C., Bick, A.G., Yu, Z., Chen, H.C., Hunt, C.M., Wendt, F., Wilson, O., Greevy, R.A., Chung, C.P., et al. (2022). APOL1 risk variants, acute kidney injury, and death in participants with african ancestry hospitalized with COVID-19 from the million veteran program. JAMA Intern. Med. *182*, 386–395. https://doi.org/10.1001/jamainternmed.2021.8538.

4. Larsen, C.P., Beggs, M.L., Saeed, M., Ambruzs, J.M., Cossey, L.N., Messias, N.C., Walker, P.D., and Freedman, B.I. (2015). Histopathologic findings associated with APOL1 risk variants in chronic kidney disease. Mod. Pathol. *28*, 95–102. https://doi.org/10.1038/modpathol.2014.92.

5. Kopp, J.B., Winkler, C.A., Zhao, X., Radeva, M.K., Gassman, J.J., D'Agati, V.D., Nast, C.C., Wei, C., Reiser, J., Guay-Woodford, L.M., et al. (2015). Clinical features and histology of apolipoprotein L1-associated nephropathy in the FSGS clinical trial. J. Am. Soc. Nephrol. *26*, 1443–1448. https://doi.org/10.1681/ASN.2013111242.

6. Ma, L., Shelness, G.S., Snipes, J.A., Murea, M., Antinozzi, P.A., Cheng, D., Saleem, M.A., Satchell, S.C., Banas, B., Mathieson, P.W., et al. (2015). Localization of APOL1 protein and mRNA in the human kidney: nondiseased tissue, primary cells, and immortalized cell lines. J. Am. Soc. Nephrol. *26*, 339–348. https://doi.org/10.1681/ASN.2013091017.

7. Scales, S.J., Gupta, N., De Mazière, A.M., Posthuma, G., Chiu, C.P., Pierce, A.A., Hötzel, K., Tao, J., Foreman, O., Koukos, G., et al. (2020). Apolipoprotein L1-specific antibodies detect endogenous APOL1 inside the endoplasmic reticulum and on the plasma membrane of podocytes. J. Am. Soc. Nephrol. *31*, 2044–2064. https://doi.org/10.1681/asn.2019080829.

8. Ma, L., Ainsworth, H.C., Snipes, J.A., Murea, M., Choi, Y.A., Langefeld, C.D., Parks, J.S., Bharadwaj, M.S., Chou, J.W., Hemal, A.K., et al. (2020). APOL1 kidney-risk variants induce mitochondrial fission. Kidney Int. Rep. *5*, 891–904. https://doi.org/10.1016/j.ekir.2020.03.020.

9. Ge, M., Molina, J., Ducasa, G.M., Mallela, S.K., Varona Santos, J., Mitrofanova, A., Kim, J.J., Liu, X., Sloan, A., Mendez, A.J., et al. (2021). APOL1 risk variants affect podocyte lipid homeostasis and energy production in focal segmental glomerulosclerosis. Hum. Mol. Genet. *30*, 182–197. https://doi.org/10.1093/hmg/ddab022.

10. Wen, H., Kumar, V., Lan, X., Shoshtari, S.S.M., Eng, J.M., Zhou, X., Wang, F., Wang, H., Skorecki, K., Xing, G., et al. (2018). APOL1 risk variants cause podocytes injury through enhancing endoplasmic reticulum stress. Biosci. Rep. *38*. https://doi.org/10.1042/bsr20171713.

11. Olabisi, O.A., Zhang, J.Y., VerPlank, L., Zahler, N., DiBartolo, S., 3rd, Heneghan, J.F., Schlöndorff, J.S., Suh, J.H., Yan, P., Alper, S.L., et al. (2016). APOL1 kidney disease risk variants cause cytotoxicity by depleting cellular potassium and inducing stress-activated protein kinases. Proc. Natl. Acad. Sci. USA *113*, 830–837. https://doi.org/10.1073/pnas.1522913113.

12. Jourde-Chiche, N., Fakhouri, F., Dou, L., Bellien, J., Burtey, S., Frimat, M., Jarrot, P.-A., Kaplanski, G., Le Quintrec, M., Pernin, V., et al. (2019). Endothelium structure and function in kidney health and disease. Nat. Rev. Nephrol. *15*, 87–108. https://doi.org/10.1038/s41581-018-0098-z.

13. Zhaorigetu, S., Wan, G., Kaini, R., Jiang, Z., and Hu, C.a.A. (2008). ApoL1, a BH3-only lipid-binding protein, induces autophagic cell death. Autophagy *4*, 1079–1082. https://doi.org/10.4161/auto.7066.

14. Nichols, B., Jog, P., Lee, J.H., Blackler, D., Wilmot, M., D'Agati, V., Markowitz, G., Kopp, J.B., Alper, S.L., Pollak, M.R., and Friedman, D.J. (2015). Innate immunity pathways regulate the nephropathy gene Apolipoprotein L1. Kidney Int. *87*, 332–342. https://doi.org/10.1038/ki.2014.270.

15. Wu, J., Ma, Z., Raman, A., Beckerman, P., Dhillon, P., Mukhi, D., Palmer, M., Chen, H.C., Cohen, C.R., Dunn, T., et al. (2021). APOL1 risk variants in individuals of African genetic ancestry drive endothelial cell defects that exacerbate sepsis. Immunity *54*, 2632–2649.e6. https://doi.org/10.1016/j.immuni.2021.10.004.

16. Menon, R., Otto, E.A., Hoover, P., Eddy, S., Mariani, L., Godfrey, B., Berthier, C.C., Eichinger, F., Subramanian, L., Harder, J., et al. (2020). Single cell transcriptomics identifies focal segmental glomerulosclerosis remission endothelial biomarker. JCI insight *5*, e133267. https://doi.org/10.1172/jci.insight.133267.

17. Sampson, M.G., Robertson, C.C., Martini, S., Mariani, L.H., Lemley, K.V., Gillies, C.E., Otto, E.A., Kopp, J.B., Randolph, A., Vega-Warner, V., et al. (2016). Integrative genomics identifies novel associations with APOL1 risk genotypes in black NEPTUNE subjects. J. Am. Soc. Nephrol. *27*, 814–823. https://doi.org/10.1681/asn.2014111131.

18. McNulty, M.T., Fermin, D., Eichinger, F., Jang, D., Kretzler, M., Burtt, N.P., Pollak, M.R., Flannick, J., Weins, A., Friedman, D.J.; Nephrotic Syndrome Study Network NEPTUNE, and Sampson, M.G. (2022). A glomerular transcriptomic landscape of apolipoprotein L1 in Black patients with focal segmental glomerulosclerosis. Kidney Int. *102*, 136–148. https://doi.org/10.1016/j.kint.2021.10.041.

19. Beckerman, P., Bi-Karchin, J., Park, A.S.D., Qiu, C., Dummer, P.D., Soomro, I., Boustany-Kari, C.M., Pullen, S.S., Miner, J.H., Hu, C.A.A., et al. (2017). Transgenic expression of human APOL1 risk variants in podocytes induces kidney disease in mice. Nat. Med. *23*, 429–438. https://doi.org/10.1038/nm.4287.

20. Marina, O.C., Sanders, C.K., and Mourant, J.R. (2012). Correlating light scattering with internal cellular structures. Biomed. Opt Express *3*, 296–312. https://doi.org/10.1364/boe.3.000296.

21. Shah, S.S., Lannon, H., Dias, L., Zhang, J.Y., Alper, S.L., Pollak, M.R., and Friedman, D.J. (2019). APOL1 kidney risk variants induce cell death via mitochondrial translocation and opening of the mitochondrial permeability transition pore. J. Am. Soc. Nephrol. *30*, 2355–2368. https://doi.org/10.1681/asn.2019020114.

22. Olabisi, O., Al-Romaih, K., Henderson, J., Tomar, R., Drummond, I., MacRae, C., and Pollak, M. (2016). From man to fish: what can Zebrafish tell us about ApoL1 nephropathy? Clin. Nephrol. *86*, 114–118. https://doi.org/10.5414/cnp86s116.

23. Chaudhary, N.S., Moore, J.X., Zakai, N.A., Judd, S.E., Naik, R.P., Limou, S., Cushman, M., Lange, L.A., Wang, H.E., Winkler, C.A., et al. (2019). APOL1 nephropathy risk alleles and risk of sepsis in blacks. Clin. J. Am. Soc. Nephrol. *14*, 1733–1740. https://doi.org/10.2215/cjn.04490419.

24. Larsen, C.P., Wickman, T.J., Braga, J.R., Matute-Trochez, L.A., Hasty, A.E., Buckner, L.R., Arthur, J.M., Haun, R.S., and Velez, J.C.Q. (2021). APOL1 risk variants and acute kidney injury in black Americans with COVID-19. J Clinical Journal of the American Society of Nephrology *16*, 1790–1796. https://doi.org/10.2215/CJN.01070121.

25. Graesser, D., Solowiej, A., Bruckner, M., Osterweil, E., Juedes, A., Davis, S., Ruddle, N.H., Engelhardt, B., and Madri, J.A. (2002). Altered vascular permeability and early onset of experimental autoimmune encephalomyelitis in PECAM-1-deficient mice. J. Clin. Invest. *109*, 383–392. https://doi.org/10.1172/jci13595.

26. Hu, M., Zhang, H., Liu, Q., and Hao, Q. (2016). Structural basis for human PECAM-1-mediated trans-homophilic cell adhesion. Sci. Rep. *6*, 38655. https://doi.org/10.1038/srep38655.

27. Kirita, Y., Wu, H., Uchimura, K., Wilson, P.C., and Humphreys, B.D. (2020). Cell profiling of mouse acute kidney injury reveals conserved cellular responses to injury. Proc. Natl. Acad. Sci. USA *117*, 15874–15883. https://doi.org/10.1073/pnas.2005477117.

28. Matsukawa, A., Lukacs, N.W., Hogaboam, C.M., Knibbs, R.N., Bullard, D.C., Kunkel, S.L., and Stoolman, L.M. (2002). Mice genetically lacking endothelial selectins are resistant to the lethality in septic peritonitis. Exp. Mol. Pathol. *72*, 68–76. https://doi.org/10.1006/exmp.2001.2416.

29. Zhang, Z., Sun, Z., Fu, J., Lin, Q., Banu, K., Chauhan, K., Planoutene, M., Wei, C., Salem, F., Yi, Z., et al. (2021). Recipient APOL1 risk alleles associate with death-censored renal allograft survival and rejection episodes. J. Clin. Invest. *131*, e146643. https://doi.org/10.1172/jci146643.

30. Liu, E., Radmanesh, B., Chung, B.H., Donnan, M.D., Yi, D., Dadi, A., Smith, K.D., Himmelfarb, J., Li, M., Freedman, B.S., and Lin, J. (2020). Profiling APOL1 nephropathy risk variants in genome-edited kidney organoids with single-cell transcriptomics. Kidney360 *1*, 203–215. https://doi.org/10.34067/kid.0000422019.

31. Nadkarni, G.N., Chauhan, K., Verghese, D.A., Parikh, C.R., Do, R., Horowitz, C.R., Bottinger, E.P., and Coca, S.G. (2018). Plasma biomarkers are associated with renal outcomes in individuals with APOL1 risk variants. Kidney Int. *93*, 1409–1416. https://doi.org/10.1016/j.kint.2018.01.026.

32. Taylor, H.E., Khatua, A.K., and Popik, W. (2014). The innate immune factor apolipoprotein L1 restricts HIV-1 infection. J. Virol. *88*, 592–603. https://doi.org/10.1128/jvi.02828-13.

33. Bundy, J.L., Anderson, B.R., Francescatto, L., Garrett, M.E., Soldano, K.L., Telen, M.J., Davis, E.E., and Ashley-Koch, A.E. (2019). RNA sequencing of isolated cell populations expressing human APOL1 G2 risk variant reveals molecular correlates of sickle cell nephropathy in zebrafish podocytes. PLoS One *14*, e0217042. https://doi.org/10.1371/journal.pone.0217042.

34. Shetty, A.A., Tawhari, I., Safar-Boueri, L., Seif, N., Alahmadi, A., Gargiulo, R., Aggarwal, V., Usman, I., Kisselev, S., Gharavi, A.G., et al. (2021). COVID-19-Associated glomerular disease. J. Am. Soc. Nephrol. *32*, 33–40. https://doi.org/10.1681/asn.2020060804.

35. Gaillard, F., Ismael, S., Sannier, A., Tarhini, H., Volpe, T., Greze, C., Verpont, M.C., Zouhry, I., Rioux, C., Lescure, F.X., et al. (2020). Tubuloreticular inclusions in COVID-19-related collapsing glomerulopathy. Kidney Int. *98*, 241. https://doi.org/10.1016/j.kint.2020.04.022.

36. Wu, H., Larsen, C.P., Hernandez-Arroyo, C.F., Mohamed, M.M.B., Caza, T., Sharshir, M., Chughtai, A., Xie, L., Gimenez, J.M., Sandow, T.A., et al. (2020). AKI and collapsing glomerulopathy associated with COVID-19 and APOL 1 high-risk genotype. J. Am. Soc. Nephrol. *31*, 1688–1695. https://doi.org/10.1681/asn.2020050558.

37. Lake, B.B., Menon, R., Winfree, S., Hu, Q., Ferreira, R.M., Kalhor, K., Barwinska, D., Otto, E.A., Ferkowicz, M., Diep, D., et al. (2021). An atlas of healthy and injured cell states and niches in the human kidney. Preprint at

bioRxiv. https://doi.org/10.1101/2021.07.28.454201 %J bioRxiv.

38. Chung, J.H., Bell, A.C., and Felsenfeld, G. (1997). Characterization of the chicken beta-globin insulator. Proc. Natl. Acad. Sci. USA *94*, 575–580. https://doi.org/10.1073/pnas.94.2.575.

39. Maresca, M., Lin, V.G., Guo, N., and Yang, Y. (2013). Obligate ligation-gated recombination (ObLiGaRe): custom-designed nuclease-mediated targeted integration through nonhomologous end joining. Genome Res. *23*, 539–546. https://doi.org/10.1101/gr.145441.112.

40. Boreström, C., Jonebring, A., Guo, J., Palmgren, H., Cederblad, L., Forslöw, A., Svensson, A., Söderberg, M., Reznichenko, A., Nyström, J., et al. (2018). A CRISP(e)R view on kidney organoids allows generation of an induced pluripotent stem cell-derived kidney model for drug discovery. Kidney Int. *94*, 1099–1110. https://doi.org/10.1016/j.kint.2018.05.003.

41. Lundin, A., Porritt, M.J., Jaiswal, H., Seeliger, F., Johansson, C., Bidar, A.W., Badertscher, L., Wimberger, S., Davies, E.J., Hardaker, E., et al. (2020). Development of an ObLiGaRe Doxycycline Inducible Cas9 system for pre-clinical cancer drug discovery. Nat. Commun. *11*, 4903. https://doi.org/10.1038/s41467-020-18548-9.

STAR★METHODS

KEY RESOURCES TABLE

REAGENT or RESOURCE	SOURCE	IDENTIFIER
Antibodies		
CD31-BV421	BD-Biosciences	564089; lot: 1307912; RRID:AB_2714010
ICAM1-FITC	R&D systems	BBA20; lot: LAA1019121; RRID:AB_356942
CD31	Abcam	ab24590; clone P2B1; lot: GR3284197-2; RRID:AB_448167
TNFRSF1A	R&D systems	AF225; RRID:AB_355201
Donkey anti-Mouse IgG (H + L) Highly Cross-Adsorbed Secondary Antibody, Alexa Fluor 647	ThermoFisher	A-31571; lot: 2260928
Chemicals, peptides, and recombinant proteins		
Halt Protease Inhibitor Cocktail	ThermoFisher	87786
Doxycycline	Sigma-Aldrich	D3447
Critical commercial assays		
Human APOL1 ELISA Kit	Proteintech	KE00047-96T
Mitophagy Detection Kit	Dojindo	MD01
Caspase-Glo 8	Promega	G8200
Caspase-Glo 3/7 assay system	Promega	G8090
XTT cell viability assay	Sigma-Aldrich	11465015001
Taqman gene expression assay for ICAM1	ThermoFisher	Hs00164932_m1
Taqman gene expression assay for PECAM1	ThermoFisher	Hs01065279_m1
Taqman gene expression assay for HPRT	ThermoFisher	Hs02800695_m1
Taqman gene expression assay for CCL2	ThermoFisher	Hs00234140_m1
Taqman gene expression assay for CCL5	ThermoFisher	Hs00982282_m1
Taqman gene expression assay for NOS3	ThermoFisher	Hs01574665_m1
Taqman gene expression assay for vWF	ThermoFisher	Hs01109446_m1
Taqman gene expression assay for APOL1	ThermoFisher	Hs01066280_m1
Pierce BCA Protein Assay Kit	ThermoFisher	23225
LysoTracker Deep Red	ThermoFisher	L12492
CD31 Micro-Bead Kit	Miltenyi Biotec	130-091-935
CellTracker Red CMTPX Dye	Invitrogen	C34552
Incucyte Annexin V Dye for Apoptosis	Sartorius	4641
STEMdiff Endothelial Differentiation Kit	Stem cell Technologies	08005
STEMdiff Mesoderm Induction Medium	Stem cell Technologies	05220
STEMdiff endothelial expansion medium	Stem cell Technologies	08007
Complete classic medium with 10% serum and CultureBoost	Cell-systems	4Z0-500
P3 Primary Cell 4D-Nucleofector X Kit L	Lonza	V4XP-3024
Cellartis DEF-CS 500 Culture System	Cellartis	Y30010
Deposited data		
10x single-cell transcriptomics data from 46 donors with CKD	Kidney Precision Medicine Project (KPMP), ref. 37	GSE183279
RNA-seq data from subjects with focal segmental glomerulosclerosis (FSGS)	McNulty et al., ref. 18	https://hugeampkpn.org/paper.html?paper=apol1_portal

(*Continued on next page*)

Continued

REAGENT or RESOURCE	SOURCE	IDENTIFIER
Ingenuity pathway analysis (IPA)	Qiagen	Software version 70750971
Experimental models: Cell lines		
Human: iPSC line N17	Boreström 2018, ref. 38	N/A
Human:Tet-ON ApoL1 G0 (wt) iPSC line	This study, clone AB4	N/A
Human:Tet-ON ApoL1 G1 iPSC line	This study, clone BD9	N/A
Human:Tet-ON ApoL1 G2 iPSC line	This study, clone AI14	N/A
Human: primary glomerular microvascular endothelial cells (HGECs)	Cell-Systems, https://cell-systems.com/	ACBRI 128; lot: 128.04.OM.01.OR
Oligonucleotides		
Forward primer "AAVS1 screen F1" to confirm correct APOL1-cassette integration in the 5'end (junction PCR): gggtcacctctcactcctttcat	Sigma-Aldrich	N/A
Reverse primer "hyg R3" to confirm correct APOL1-cassette integration in the 5'end (junction PCR): atttacccgcaggacatatccac	Sigma-Aldrich	N/A
Forward primer "CAGR3" to confirm correct APOL1-cassette integration in the 3'end (junction PCR): tggcgttactatgggaacatacg	Sigma-Aldrich	N/A
Reverse primer "AAVS1 R5" to confirm correct APOL1-cassette integration in the 3'end (junction PCR): ccagatagcactggggactcttt	Sigma-Aldrich	N/A
Forward primer "AP6_fw" to confirm correct inserted APOL1-sequence: GAGCCAGAGCCAATCTTCAGT	Sigma-Aldrich	N/A
Reverse primer "AP7_rev" to confirm correct inserted APOL1-sequence: GCGGAATAGGAACTAAGGAGGAT	Sigma-Aldrich	N/A
Recombinant DNA		
Tet-ON ApoL1 G0 (wt) cDNA	GeneArt; Table S3	N/A
Tet-ON ApoL1 G1-cDNA with the S342G and I384 M-mutations	This work, Table S3	N/A
Tet-ON ApoL1 G2-cDNA deleted for Asn 388 and Tyr 389	This work, Table S3	N/A
pIRES-hrGFP-1a-vector	Agilent	240031
His-tagged APOL1 G0 construct for electroporation	Table S8	N/A
His-tagged APOL1 G1 construct for electroporation	Table S8	N/A
Software and algorithms		
NephroSeq v4	https://www.nephroseq.com/resource/login.html.	N/A
GraphPad Prism 8	GraphPad	N/A
DNASTAR Molecular biology-suite 17.3.057	DNASTAR	N/A
Columbus 2.9.1	PerkinElmer	N/A
FlowJo 10.8.0	Flowjo	N/A
Incucyte 2021A	Sartorius	N/A
Seahorse Wave 2.6.1 Desktop Software	Agilent	N/A

RESOURCE AVAILABILITY

Lead contact

Miguel Carracedo Ortiz (miguel.carracedoortiz@astrazeneca.com)

Materials availability

Further information and requests for resources, plasmids, cell lines and reagents generated in this study should be directed to and will be fulfilled by the lead contact.

Data and code availability

- Single-cell RNA-seq data and RNA-seq data analyzed in the current study are publicly available at GEO. Accession numbers are listed in the key resources table. The DOI is listed in the key resources table. Microscopy data reported in this paper will be shared by the lead contact upon request.
- This paper does not report original code.
- Any additional information required to reanalyze the data reported in this paper is available from the lead contact upon request.

MATERIAL AND METHODS

Bioinformatic analysis

10x single-cell transcriptomics generated within the Kidney Precision Medicine Project (KPMP) integrated in total 46 donors with CKD (diabetic kidney disease and hypertensive nephropathy), AKI or healthy (GSE183279).[37] Age, sex and eGFR are described in Tables S2A and S2B. The full dataset, containing cohort characteristics can be found at: https://www.kpmp.org/doi-collection/10-48698-3z31-8924. The processing largely followed the standard integration pipeline for Seurat 3, using the SCT normalization path. The fraction of mitochondrial reads was very high for a large proportion of the samples, indicating low quality. A generous cutoff of 30% was therefore applied. Donors with <1000 cells passing QC were excluded. Gene expression data from a nephrotic syndrome cohort with varied histologic diagnoses was accessed and analyzed using NephroSeq v4 https://www.nephroseq.com/resource/login.html.

RNA-seq data from subjects with focal segmental glomerulosclerosis (FSGS) was analyzed by McNulty et al.[18] and downloaded from https://hugeampkpn.org/paper.html?paper=apol1_portal. Downstream analysis of the data was performed utilizing Ingenuity pathway analysis (IPA), version 70750971, between 2021-01 and 2021-03. The dataset of transgenic mice overexpressing APOL1 under the nephrin promoter from Beckerman P et al.[19] is integrated within the Qiagen OmicSoft Suite, and available for pathway analysis in IPA. Gene expression, pathway, upstream regulator, and comparison analyses were performed utilizing IPA. For comparison analysis, a threshold of 2 log(10) was used to determine not significantly enriched pathways within the datasets.

Target vector design inducible ApoL1

Three CDS sequences, 1242 bp in length for ApoL1 wt and G1 and 1236 bp CDS for the G2 variant were synthesised at GeneArt and fused to the bGlopA sequence.

The desired point mutations for G1 (S342G and I384 M) and G2 (deleted for Asn 388 and Tyr 389) were introduced in the synthesized CDS sequences (Table S3). Each of the ApoL1 constructs were cloned into a Doxycycline-inducible vector with the CAG promoter driving the nls Tet-on 3G Tet suppressor followed by an SV40 poly Adenylation signal. The pTRE3G Tet response element driving the expression of the three ApoL1 variants and a beta globin poly adenylation signal was surrounded by a 1.2 kb insulator, CTCF, binding sites, derived from the chicken beta globin locus,[38] as schematically shown in Figure S6. The target vectors were designed to harbor ObLiGaRE sites[39] for the AAVS1 locus, PPP1R12C, to facilitate integration of the ApoL1 inducible construct's into intron 1 of PPP1R12C. A hygromycin selection cassette was included for positive selection in iPS cells. The cell lines were confirmed using three independent methods (junction PCR, droplet digital PCR (ddPCR) and sequencing as described below.

EXPERIMENTAL MODEL AND SUBJECT DETAILS

Primary cell cuture

iPSC line generation

To generate the ApoL1 G0, G1 and G2 expressing lines, the parental iPSC line N17 (generated as described by Boreström et al.[40]) was transfected with the ObLiGaRe system and Zn-finger nucleases as previously described[41] to insert the doxycycline inducible ApoL1 expression cassette (see above) containing coding

sequences of APOL1 G0, G1 and G2 (Table S3, Figures S6, and S7). The corresponding protein sequences of the inserted APOL1-cassettes are indicated in Table S4.

To generate the DNA complex for transfection, two tubes were prepared separately: tube A with 250 μL Optimem (Gibco, cat no 31985062), 5 μL PLUS reagent (Gibco, cat no 11514015) and plasmid DNA at a 1:1 M ratio of the Zn-finger vector and Donor vector (5 μg DNA in total); tube B with 250 μL Optimem and 15 μL Lipofectamine LTX (Gibco, 15338100). The reagents were incubated separately for 5 min at room temperature. The content of tubes A and B were then mixed carefully to obtain a final DNA to lipofectamine ratio of 1:3 and allowed to incubate for 5 min at room temperature. The transfection reagent was added dropwise to one well of a 6-well plate (Corning, cat no 3516) that had been pre-coated for 30 min at 37° with DEF-CS coating (Cellartis, cat no Y30010) diluted 1:10 in DPBS (Gibco, cat no 14040133). The transfection mix was incubated for 30 min at 37°.

Parental iPSC line N17-cells were cultured in the DEF-CS culture system (Cellartis, cat no Y30010) according to manufacturer's instructions and passaged every 3–4 days. On the day of transfection (day 0), cells were harvested at 80% confluence. For detachment, cells were washed with PBS (Gibco, 70011044) and incubated with TrypLESelect (Gibco, 12563029) for 5 min at 37°C. Detached cells were added to the pre-incubated transfection complex in the 6 well plate at 100,000 cells/cm2 in a final volume of 3 mL/well.

Culture medium was changed on day 1. Transfected cells were detached on day 2 as described above, and reseeded in DEF-CS coated 24-well plates (Corning, 3524) at 30,000 cells/cm2. From day 3, Hygromycin B (Gibco, 10687010) was added to the culture medium at 10 μg/ml to select for cells which had integrated the construct. On day 17, cells were passaged, and a sample was removed for editing analysis as described below. Positive pools (insert copy number below 3) of cells surviving hygromycin selection were combined and seeded as single cells in 384-well plates using limiting dilution. The existence of only one cell in the well was confirmed using a phase microscope (Incucyte S3, Sartorius). As the wells became confluent, individual cell lines were cherry-picked and transferred to a 96-well plate for propagation, followed by a split to an analysis plate and a cryopreservation plate. Clone screen was done by repeating the junction PCR and ddPCR-analysis (see below) on monoclonal lines. Clones positive in both junction PCR's and with a low copy number of the hygromycin gene were identified. The selected clones for the respective construct were expanded and cryopreserved in FBS (Gibco, 16141079), 20% DMSO (Sigma-Aldrich, cat no D2650) and 10 μM Y27632 (Millipore, cat no 688000).

Cell line confirmation - Junction PCR

To identify monoclonal cell lines carrying the intended genetic modification junction PCR was performed. We lysed the cells using 40 μL lysis buffer per well in 96-well format. The lysis buffer was added to the well in the 96-well plate and consisted of MGB, 0.01% SDS (Life Technologies AM9822) and 0.1 mg/mL proteinase K (Sigma P6556). MGB consisted of 670 mM Tris-HCl, pH 8.8, 166 mM ammonium sulfate, 65 mM MgCl2. After 1h lysis at 37°C, the lysates were transferred to an Axygen 96-well PCR-plate followed by heat inactivation at 85°C for 10 min.

The lysate was diluted 5x in nuclease-free water. Junction PCR was performed at the 5'junction and 3'junction respectively by setting up 10 μL PCR-reactions containing Extensor PCR Mastermix (ThermoFisher AB-0792/B), 500 nM forward primer, 500 nM reverse primer and 1 μL lysate using thermocycling steps indicated in Table S5. For the 5'-junction, "AAVS1 screen F1" forward primer was used with "hyg 3" reverse primer (STAR table). For the 3'-junction, "CAGR3" forward primer and "AAVS1" reverse primer (STAR table) were used. The PCR-products were run on a 1.2% agarose gel (SeaKem agarose, Lonza 50004) stained with Midori Green advanced DNA-stain (Genetics MG04) to identify cell lines generating PCR-products of the expected size (1049 bp for the 5' junction, and 867 bp for the 3' junction).

Cell lines with correct transgene cassette integration were scaled up and further tested as described below.

Cell line confirmation – ddPCR & sequencing

The lysate was prepared as described above and diluted 5x in nuclease-free water. We used a FAM-labeled Copy Number Variation ddPCR-assay to detect the hygromycin resistance gene (Bio-RAD 10031277) and a HEX-labeled reference gene assay detecting AP3B1 (Bio-RAD 10031244).

A Mastermix was prepared using a final concentration of 1x ddPCR Supermix for Probes, no dUPT (186–3024, Bio-Rad), 1x FAM-labeled assay, 1x HEX labeled reference assay, 1/40 HaeIII (15205016, Invitrogen) in ultrapure RNase and DNase free water (Invitrogen 10977-035). After adding 5 μL lysate to the 15 μL Mastermix in the semi-skirted 96-well plate (Eppendorf 30129504) followed by careful mixing, a seal (Bio-RAD 18114040) was put on the plate using a PX1 PCR Plate Sealer (Bio-RAD, cat no. 181–4000). An automated Droplet Generator (Bio-RAD) was used to generate droplets in a semi-skirted 96-well PCR plate (Eppendorf 30129504). The PCR plate was sealed as described above and placed in a C1000 Touch Thermal Cycler (Bio-RAD 185-1197) for PCR amplification using the thermocycling steps indicated in Table S6. The droplet reading was performed with the QX 100 Droplet reader (Bio-RAD 186-3001) using ddPCR Droplet Reader Oil (Bio-RAD 186-3004).

Data acquisition and analysis was performed using the software QuantaSoft (Bio-Rad) and the "CNV2" program (two copies of the reference gene AP3B1 exist in iPSC-cells). The fluorescence amplitude threshold was set manually as the midpoint between the average fluorescence amplitude of the four droplet clusters. The same threshold was applied to all the wells of the ddPCR plate. The selected lines G0 (AB4), G1 (BD9) and G2 (AI14) contained 1, 2 and 3 transgene copies, respectively. These cell lines were further characterized by sequencing, using 625 nM forward and reverse primers (AP6_fw and AP7_rev, STAR-table), Extensor Hi-Fidelity PCR Mastermix (ThermoFisher AB0792) and thermocycler program show in Table S7. The amplified PCR-products were purified using Qiaquick PCR purification kit (Qiagen 28104). Sequencing reactions were performed using the BigDye Terminator v3.1 Cycle Sequencing kit (ThermoFisher 4337456) and 350 nM forward primer (AP6_fw, STAR-table) or 350 nM reverse primer (AP7_rev, STAR-table). Sequencing confirmed perfect sequence match for all three cell lines, including the expected differences in sequence at the 3′ end of the inserted APOL1-cassettes harboring the G1 and G2-mutations (Figure S7).

Cell culture and iPSC differentiation to endothelial cells

iPSC differentiation to endothelial cells (EC's) was performed utilizing the STEMdiff Endothelial Differentiation Kit (Stem cell Technologies, 08005) according to manufacturer's instructions. In brief, iPSCs were grown in Cellartis DEF-CS 500 Culture System and seeded at 7.5E4 cells/cm2 in Cellartis DEF-CS 500 COAT-1 (Cellartis, Y30010). 24h after seeding, cells were grown in STEMdiff Mesoderm Induction Medium mesoderm induction for 48h, followed by STEMdiff Endothelial Induction Medium. After 4 days cells were detached and plated in ACF Cell Attachment Substrate (Stem cell Technologies) and grown in STEMdiff endothelial expansion medium. Differentiated cells were subsequently purified using the CD31 MicroBead Kit (Miltenyi Biotec, 130-091-935). CD31-positive cells were used for experiments. They were cultured in vessels coated with ACF Cell Attachment Substrate and grown in STEMdiff endothelial expansion medium (Stem cell Technologies, 08007).

Human primary glomerular microvascular endothelial cells (HGECs, Cell-Systems) were cultured utilizing complete classic medium with 10% serum and CultureBoost (Cell systems, 4Z0-500) according to the supplier's specified protocol. The HGECs were cultured up to passage 8.

METHOD DETAILS

Generation of plasmids expressing his-tagged APOL1 and electroporation

The pIRES-hrGFP-1a plasmid (Agilent 240031) was used both as the control plasmid and to generate plasmids expressing His-tagged APOL1 G0 or His-tagged APOL1 G1 (Table S8).

To prepare for electroporation, human glomerular endothelial cells (HGECs) were seeded in T-150 cm^2 flasks, grown overnight, and detached as described above. 6 E^5 HGECs were resuspended in 100 μL P3 electroporation buffer (Lonza, V4XP-3024) containing 0.5ug of plasmid, and placed in 100 μL cuvettes (Lonza). After electroporation using a 4D-Nucleofector X Unit (Lonza, AAF-1003X) and program DY-138-AA, cells were seeded in plates pre-coated with attachment factor (Cell-systems, 4Z0-201) and pre-warmed complete classic medium with 10% serum and CultureBoost (Cell-systems, 4Z0-500). The plates were incubated overnight in a humidified atmosphere containing 5% CO2 at 37°C. Cells were subsequently assayed at the indicated time points.

Immunofluorescence

For immunofluorescence cells were seeded in black clear bottom 96 well plates (PhenoPlate 96-well, Perkin Elmer, 6055302), treated as described in the figure legends and fixed 15min in 4% formaldehyde and washed twice with PBS (Gibco, 14190094). Fixed cells were blocked with 5% FBS (Gibco, 10500-064) in PBS followed by incubation with primary antibodies overnight detecting CD31 (Abcam, ab24590, clone P2B1) or TNFRSF1A (R&D systems, AF225). After washing with PBS (Gibco, 14190094), cells were incubated with secondary antibodies (STAR Methods table) and nuclei stained with Hoechst 33342 (Invitrogen, H3570). Confocal images were obtained using a CellVoyager CV7000 high-throughput microscope (Yokogawa). Images were analyzed utilizing the Columbus 2.9.1 software (PerkinElmer).

Protein extraction and ELISA

Cell lysates were obtained from cells washed with cold PBS (Gibco, 14190094) and lysed with RIPA buffer (Sigma-Aldrich, R0278) supplemented with Halt Protease Inhibitor Cocktail (Thermo Scientific, 87786). Protein concentrations were determined using Pierce BCA Protein Assay Kit (Thermo Scientific, 23225). APOL1 protein concentration was determined using the Human APOL1 ELISA Kit (Proteintech, KE00047) according to manufacturer's instructions.

Gene expression analysis

Reverse-transcription was performed using High-Capacity RNA-to-cDNA Kit (Applied Biosystems). Quantitative real-time PCR reaction was developed on a Quantstudio 7 Flex Fast Real-Time PCR system (Life Technologies) using Taqman Assay-on-Demand from Life Technologies. Assay ID's can be found in the STAR Methods table. The relative mRNA expression of the target genes was quantified by the 2-ΔCT or 2-ΔΔCT method using Hypoxanthine-guanine phosphoribosyltransferase (HPRT) as endogenous control.

Lysotracker labeling

Acidic vesicles were labeled using Lysotracker DeepRed (ThermoFisher L12492) according to manufacturer's instructions. In brief, after cell treatment or electroporation, cells were incubated for 30 min at 37C with 50 nM Lysotracker. After incubation, loading media was replaced with fresh media for live cell imaging or cells washed with PBS (Gibco, 14190094) and detached for flow cytometry analysis.

Macrophage attachment assay

For attachment assays, iECs and electroporated HGECs were seeded at a 3*10^4 cells/cm2 in black clear bottom 96 well plates (Perkin Elmer, 6055302). 24h after seeding, THP-1 cells, at a concentration of 0,5*10^5 cells/mL, were stained with 2uM CellTracker Red CMTPX Dye (Invitrogen, C34552) at 37C for 30min. After incubation, THP-1 cells were washed three times in PBS and resuspended in RPMI (Gibco, 61870010) with 10% heat inactivated FBS (Gibco, 10500-064) and 2 mM pyruvate (Gibco, 11360070) to a concentration of 3*10^5 cells/ml. HGECs media was removed, cells washed and 3*10^4 THP-1 in suspension added to the HGECs. THP-1 and HGECs were incubated for 45 min at 37C. After incubation, cells were washed three times with PBS. Live-cell imaging was performed using an Incucyte SX5 (Sartorius). Images were analyzed with the Incucyte 2021A software (Sartorius) utilizing both size exclusion and fluorescence to discern THP-1 cells from HGECs.

Mitophagy detection assay

Mitophagy was detected utilizing the Mitophagy Detection Kit (Dojingo MD01) according to manufacturer's instructions. Cells were washed with serum free media, pre-loaded with the Mtphagy Dye at 37C for 30min, washed and incubated with doxycycline for 24h. After 24h incubation live-cell imaging was performed in a CellVoyager CV7000 high-throughput microscope.

Flow cytometry analysis

For flow cytometry analysis cells were washed with PBS and detached with TrypLE Express (Gibco). TrypLE neutralized with complete media and cells were centrifuged for 5 min at 300g. Cells were resuspended in blocking buffer (PBS without calcium and magnesium, 2.5 mM EDTA, 5% FBS) for 15min, centrifuged and subsequently stained for 45 min at 4C with antibodies CD31-BV421 (BD-biosciences), ICAM1-FITC (R&D) and respective isotype controls according to manufacturer's indications. Samples were acquired with a BD LSR Fortessa 4L (BD-biosciences) flow cytometer and analyzed with FlowJo 10.8.0 software.

Oxygen consumption measurements

For oxygen consumption rate (OCR) analysis of live ECs were analyzed using an XF-96 Extracellular Flux Analyzer (Agilent Technologies). Cells were plated in XF-96 cell culture plates 5*10^4 cells/cm2 and treated with or without doxycycline (Sigma-Aldrich, D3447) for 24h. After treatment, cells were washed and incubated for 45min in a non-CO2 incubator with XF DMEM (Agilent Technologies) supplemented with 1 mM pyruvate, 2 mM glutamine and 10 mM glucose. Following incubation OCR was analyzed under basal conditions and after to 2 μM oligomycin, 200 μM 2,4-dinitrofenol (DNP) and 1 μM rotenone plus 1 μM antimycin A. Analysis was performed utilizing Seahorse Wave 2.6.1 Desktop Software (Agilent)

Scratch wound assay

For scratch wound assays, cells were plated in Incucyte Imagelock 96-well Plate (Sartorius) at 2.5*10^4 cells/cm2. The following day cells were treated with doxycycline (Sigma-Aldrich, D3447) for 24h and scratch wound performed utilizing Incucyte 96-well Woundmaker Tool (Sartorious). After wound cells were washed twice with PBS to remove cell debris, and media containing doxycycline or control media added. Cells were imaged using an Incucyte S3, and images analyzed utilizing the Incucyte 2021A software (Sartorius) with the IncucyteScratch Wound Analysis Software Module (Sartorius).

Caspase and cell viability analysis

Caspase-Glo 8 a(Promega G8200), Caspase-Glo 3/7 assays (Promega G8090) and XTT cell viability-assay (Sigma-Aldrich 11465015001) were performed according to manufacturers instructions. In brief, Caspase 8 and caspase 3/7 activity were measured in in 96-well plates (Falcon) according to manufacturer's recommendations. Luminescence was measured utilizing a Spectramax iD3 multi-mode microplate reader (molecular devices). Cell viability was measured colorimetrically utilizing the XTT reagent (Sigma-Aldrich, 11465015001) following manufacturer's instructions with absorbance measured in a Spectramax iD3 multi-mode microplate reader (Molecular Devices). Apoptosis was assesed utilizing Incucyte Annexin V Dye for Apoptosis (Sartorius, 4641) imaged using an Incucyte S3, and images analyzed utilizing the Incucyte 2021A software (Sartorius).

QUANTIFICATION AND STATISTICAL ANALYSIS

Results are expressed as either mean ± S.D. or mean with 95% CI. Results are shown as fold change compared with controls for semi-quantitative mRNA and protein analyses of paired experiments to account for unwanted sources of variation, indicated as fold change on the y axis. In each experiment, biological repeats were performed to ensure consistent responses in experiments. No exclusion of outliers was performed in the data analysis of the present study. Normality was assesed utilizing shapiro-wilk test of normality. Statistical significance of differences between groups for normally distributed data was assessed with Student t test when comparing two groups and with one-way or two-way ANOVA as appropriate followed by Tukey's post hoc tests for multiple comparisons only if F was significant and there was no variance in homogeneity. Statistical significance was assigned at $p < 0.05$, and statistical difference levels were assigned as follows in the Figures, *$p < 0.05$, **$p < 0.01$, ***$p < 0.001$, ****$p < 0.001$. Statistical analysis was performed using GraphPad Prism 9 (GraphPad Software Inc, CA, USA).